Single-molecule microscopy reveals membrane microdomain organization of cells in a living vertebrate

Schaaf, M.J.M.; Koopmans, W.; Meckel, T.M.; Noort, S.J.T. van; Snaar, B.E.; Schmidt, T.; Spaink, H.P.

Single-Molecule Microscopy Reveals Membrane Microdomain Organization of Cells in a Living Vertebrate

Marcel J. M. Schaaf,[†*] Wiepke J. A. Koopmans,[‡] Tobias Meckel,[‡] John van Noort,[‡] B. Ewa Snaar-Jagalska,[†] Thomas S. Schmidt,[‡] and Herman P. Spaink[†]
[†]Molecular Cell Biology, Institute of Biology, and [‡]Physics of Life Processes, Institute of Physics, Leiden University, Leiden, The Netherlands

ABSTRACT It has been possible for several years to study the dynamics of fluorescently labeled proteins by single-molecule microscopy, but until now this technology has been applied only to individual cells in culture. In this study, it was extended to stem cells and living vertebrate organisms. As a molecule of interest we used yellow fluorescent protein fused to the human H-Ras membrane anchor, which has been shown to serve as a model for proteins anchored in the plasma membrane. We used a wide-field fluorescence microscopy setup to visualize individual molecules in a zebrafish cell line (ZF4) and in primary embryonic stem cells. A total-internal-reflection microscopy setup was used for imaging in living organisms, in particular in epidermal cells in the skin of 2-day-old zebrafish embryos. Our results demonstrate the occurrence of membrane microdomains in which the diffusion of membrane proteins in a living organism is confined. This membrane organization differed significantly from that observed in cultured cells, illustrating the relevance of performing single-molecule microscopy in living organisms.

INTRODUCTION

Studying the dynamics of individual molecules in living cells provides a wealth of knowledge about processes that take place at the plasma membrane. Application of this technology provides detailed insight into the diffusion patterns of specific molecules and, therefore, into the organization of the plasma membrane. For example, the occurrence of membrane microdomains that confine the diffusion of molecules in the membrane is revealed, and a detailed view of alterations in these domains during signal transduction processes is provided.

Investigation of the diffusion patterns of individual molecules in the plasma membrane of a living cell is performed in two ways. First, single-particle tracking is performed using gold-labeled membrane proteins or lipids (for a review, see Kusumi et al. (1)). Second, using fluorescent labeling techniques, molecules are imaged and tracked using a laser-based fluorescence microscopy setup equipped with a high-sensitivity CCD camera (2). The labeling of proteins and lipids is achieved using small organic fluorescent dye molecules (3,4) or applying autofluorescent proteins, such as green fluorescent protein (GFP), genetically fused to an endogenous protein (5). Application of this technique has provided insight into the diffusional properties of a wide variety of membrane-bound proteins (6–10) at a time resolution of ~5 ms and a positional accuracy of ~40 nm in most studies.

Until now, all single-molecule microscopy studies on living cells have been performed in cultured eukaryotic cells. It is likely that the molecular diffusion pattern and membrane organization observed in these cells does not reflect the situation in cells that constitute a specific tissue in a living multicellular organism. To measure molecular dynamics in a physiologically relevant system, we have extended the application of single-molecule microscopy to the level of a living vertebrate organism. This also enables the validation of previous findings in an in vivo model system and makes it possible to investigate the behavior of individual signaling molecules in relation to processes like development and pathogenesis of various diseases.

The zebrafish was used as a model system in this study. Zebrafish embryos have been shown to be suitable model organisms for in vivo fluorescence microscopy studies, because they are small, transparent, and easy to manipulate. They have been used for real-time imaging of GFP-labeled cells in vivo (11,12). Even dynamic processes at the subcellular level have been imaged using GFP tagging of specific proteins in a living embryo (13).

We chose as a fluorescent molecule of interest yellow fluorescent protein (YFP) fused to the membrane anchor of the human H-Ras protein, which is a member of the Ras family of small GTPases. This protein family plays a key role in tyrosine-kinase-receptor-induced signaling that controls cell growth, differentiation, and survival (14). The fusion protein used in this study, YFP-C10H-Ras, consists of the YFP and the 10 most C-terminal amino acids of human H-Ras fused to the YFP C-terminus. These 10 amino acids constitute a signal for the posttranslational addition of three lipid groups that anchor this protein in the cytoplasmic leaflet of the plasma membrane. In a previous study, the diffusion pattern in YFP-C10H-Ras was studied in detail using single-molecule microscopy (15), which showed diffusion behavior similar to that of the human Lck and K-Ras membrane anchors (16) and the activated full-length H-Ras protein fused to YFP (10). This molecule therefore serves as a model molecule for proteins anchored in the cytoplasmic

Submitted December 23, 2008, and accepted for publication May 22, 2009.

*Correspondence: m.j.m.schaaf@biology.leidenuniv.nl

Editor: Gerard Marriott.

0006-3495/09/08/1206/9 $2.00

doi: 10.1016/j.bpj.2009.05.044

leaflet of the plasma membrane, and because it is biologically inert, it serves as a probe for the detection of changes in the organization of the plasma membrane.

In this study, using the zebrafish as a model system and YFP-C10H-Ras as a molecule of interest, we demonstrate that it is possible to perform single-molecule microscopy in a living vertebrate organism. We investigated YFP-C10H-Ras in three systems: in vitro (a cell line), ex vivo (embryonic stem cells), and in vivo (epidermal cells of 2-day-old embryos). Our results demonstrate that in these cell types there are large differences between the membrane domains in which the YFP-C10H-Ras molecules are confined.

MATERIALS AND METHODS

Zebrafish, mRNA microinjection and primary cell cultures

Zebrafish

Wild-type zebrafish (*Danio rerio*) were maintained according to standard protocols (http://ZFIN.org) on a 14-h light, 10-h dark photoperiod cycle at 28°C. Embryos were obtained by natural crosses. Fertilized eggs were collected and raised in egg water (60 μg/ml Instant Ocean sea salts (Aquarium Systems, Mentor, OH)) at 28°C. All procedures in this study that involve animals are in compliance with local animal welfare regulations and were approved by the local animal welfare committee.

Microinjection of mRNA in zebrafish eggs

Synthesis of YFP-C10H-Ras mRNA was performed using the mMessage mMachine high-yield capped RNA transcription kit (Ambion, Austin, TX) according to the manufacturer's instructions and using PCS2+-YFP-C10H-Ras as a template. The resulting mRNA was purified using the RNeasy mini kit (Qiagen, Venlo, The Netherlands), and was microinjected into zebrafish eggs at the one- to two-cell stage (30 pg/egg). Microinjection was controlled by a stereomicroscope, a Femtojet microinjector (Eppendorf, Hamburg, Germany), and a micromanipulator with pulled microcapillary pipettes. Injected eggs were then allowed to develop in egg water at 28°C.

Primary cell cultures

Primary embryonic cell cultures were made by dissociation of embryos between 3.5 and 4 h after fertilization. Dissociation was performed by suspending the embryonic cells in a calcium/magnesium-free solution (60 mM NaCl, 4 mM KCl, 5 mM $NaHCO_3$, pH 7.0) using a Pasteur pipette. The suspension was transferred to a 1.5-ml Eppendorf tube and spun down for 5 min at 3000 rpm. The cells were resuspended in phosphate-buffered saline, transferred to four-well slides (Nunc, Roskilde, Denmark), and maintained at room temperature. Between 1 and 3 h after starting the culture, cells were used for single-molecule microscopy.

Cells and transfection

ZF4 cells

ZF4 cells were grown and transfected as described previously (17). Briefly, they were grown at 28°C in Ham F12 medium (Invitrogen, Carlsbad, CA) and 10% fetal calf serum (Invitrogen).

Cell transfection

Generation of the expression plasmid pcDNA3.1-YFP-C10H-Ras has been described previously (16). For our purposes, the YFP-C10H-Ras sequence was transferred from this vector into the plasmid PCS2+ (see http://sitemaker.u-mich.edu/dlturner.vectors/home) using the *Bam*HI and *Xho*I restriction sites. This resulted in the plasmid PCS2+-YFP-C10H-Ras, which was used in this study.

Transfection of this plasmid into ZF4 cells was performed by nucleofection using the Cell Line Nucleofector kit V (Amaxa, Cologne, Germany) according to the manufacturer's instructions. After nucleofection, cells were transferred into four-well slides (Nunc). Cells were used for single-molecule microscopy between 4 and 5 days after transfection. Before measurements were made, the medium was replaced by room-temperature phosphate-buffered saline (150 mM NaCl, 10 mM Na_2HPO_4/NaH_2PO_4, pH 7.4) and cells were equilibrated at this temperature for 10 min.

Microscopy

Wide-field microscopy

For wide-field imaging, we used an Axioplan Imaging 2 microscope with differential interference contrast equipped with an AxioCam MRc5 camera (Zeiss, Jena, Germany) (see Fig. 3 *B*) or a Leica MZ16FA microscope equipped with a DFC420C camera (Leica Microsystems, Wetzlar, Germany) (see Figs. 3 *A* and 5, *A–D*).

Confocal laser-scanning microscopy

Two different microscope systems were used for confocal laser scan images. For some images, we used a Leica SP1 confocal laser scanning microscope (Leica Microsystems) (see Figs. 1 and 3 *E*). Excitation was done with an argon laser at 514 nm. Images were captured using a 63× water immersion objective. For other images, we used a BioRad MRC 1024 ES confocal laser scanning microscope (BioRad, Hercules, CA) (see Figs. 3, *C* and *D*, and 5, *E–G*, and Fig. S2 in the Supporting Material). Excitation was done with an argon laser at 514 nm, and images were taken using a 10×, 20×, or 40× objective.

Single-molecule microscopy

Wide-field fluorescence microscopy

Cultured ZF4 cells and primary cells were studied by single-molecule microscopy using a wide-field fluorescence microscopy setup described previously (2,5,15). The microscope (Axiovert 100TV, Zeiss) was equipped with a 100× oil-immersion objective (NA 1.4; Zeiss). A region-of interest was set to 50 × 50 pixel at a pixel size of 220 nm. Excitation was done using a 514-nm argon laser line (Spectra Physics, Mountain View, CA) combined with an acoustooptic tunable filter, which illuminated the region of interest for 3 ms with a power of ~2 kW/cm^2. The time lag between subsequent illuminations was varied between 6.25 and 75 ms. The camera frame rate was synchronized with the action of the acoustooptic tunable filter. Fluorescent light was filtered by a combination of filters (DCLP530 and HQ570/80 from Chroma Technology (Brattleboro, VT) and OG530-3 from Schott (Mainz, Germany)) and detected by a liquid-nitrogen-cooled slow-scan charge-coupled device (CCD) camera (Princeton Instruments, Trenton, NY). Measurements were performed at room temperature.

Total internal reflection fluorescence microscopy

Cleaned coverslips were coated with 50 μg/ml poly-D-lysine (Sigma, St. Louis, MO) for 5 min. A 2-day-old zebrafish embryo (between 50 and 55 h postfertilization, equilibrated at room temperature for at least 1 h) was placed on its side on the coverslip in a drop of egg water. A sheet of agarose (2%) 0.75 mm thick was placed over the embryo covering the tail region. The coverslip was mounted on a total internal reflection fluorescence (TIRF) microscopy setup that has been described previously (18). It consists of a home-built microscope equipped with a 100× oil-immersion TIRF objective (NA 1.45, Nikon, Tokyo, Japan). A 200 × 200-pixel region of interest was defined at a pixel size of 213 nm. Excitation was done using a 514-nm Argon laser (Coherent, Santa Clara, CA) line, illuminating an area of

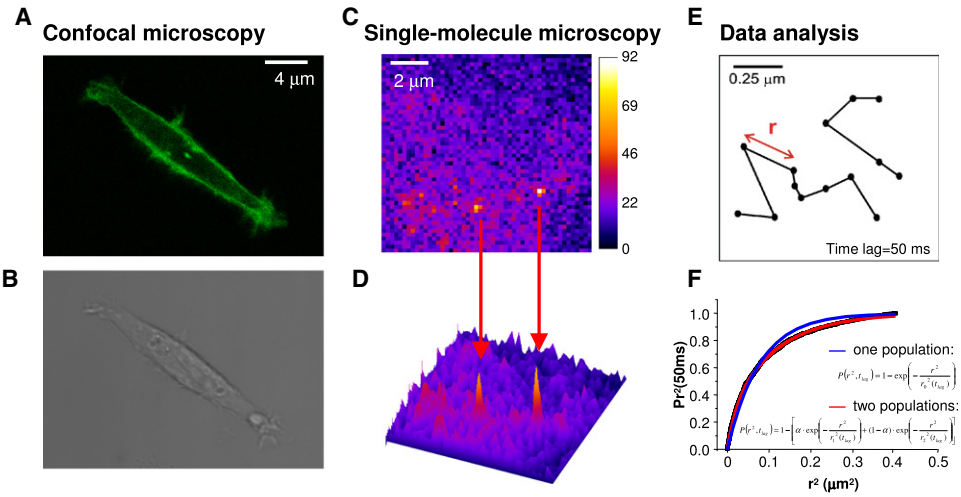

FIGURE 1 Single-molecule microscopy images of the diffusion behavior of YFP-C10H-Ras in ZF4 cells. (*A*) Subcellular localization of YFP-C10H-Ras in cultured zebrafish cells. Cells from the ZF4 cell line (zebrafish embryonic fibroblast cells) were transiently transfected with a YFP-C10H-Ras expression plasmid, and localization of the fluorescent signal was visualized using confocal laser scanning microscopy. The image shows that the vast majority of fluorescence is localized at the plasma membrane. (*B*) Bright-field image of the same cell showing the outline of the cell. (*C*) Single-molecule microscopy of YFP-C10H-Ras molecules in the membrane of ZF4 cells. Image of the apical membrane of a YFP-C10H-Ras-expressing ZF4 cell. (*D*) Three-dimensional representation of fluorescence intensities of the image in *C*. Two fluorescence-intensity peaks that can be attributed to a single YFP molecule are shown. (*E*) Examples of trajectories found for several YFP-C10H-Ras molecules in the apical membrane of the cell shown in *A*. (*F*) Representative cumulative distribution plot of squared displacements. Between 200 and 3000 trajectories of individual molecules were analyzed and the squared displacement was calculated for each step of these trajectories. The obtained squared displacements were plotted as shown in this example, displaying 2304 data points derived from an experiment in which a time lag of 50 ms was used (*black squares*). The data were fitted using a biexponential probability function, and the fitted curve is shown in red. The fitting results indicated the occurrence of two subpopulations of molecules, and made it possible to determine the relative size of the subpopulations (α) and their mean-squared displacements ($r^2{}_1$ and $r^2{}_2$). This procedure was performed for each time lag used.

~600 μm^2 with a power of 0.9 mW. The beam was circularly polarized and displaced parallel to the optical axis of the objective, so an evanescent wave was generated by total internal reflection of the laser light at the glass-water interface. Excitation intensity at the interface was estimated to be ~0.6 kW/cm^2. Fluorescence light was filtered using a custom-made dual-color bandpass filter (Chroma), and by a long-pass filter (OG530, Schott). Images were collected by a multiplication-gain CCD camera (Cascade 512B, Roper Scientific, Trenton, NJ).

Analysis of YFP-C10H-Ras diffusion

Analysis of the position of individual molecules and their movements between consecutive images was done as described previously (15,19). The signals attributed to individual molecules were fitted to a two-dimensional Gaussian surface, permitting the localization of the molecule with a positional accuracy that is determined by the quotient of the full-width-at-half-maximum of the Gaussian fit and the square root of the number of photons detected (20). By connectivity analysis between consecutive images, the two-dimensional trajectories of the molecules and their squared displacements (r^2) were determined for each time lag used. The determined positional accuracy (dx) led to a constant offset in $r_i{}^2$ of $4\cdot(dx)^2$. Since the trajectories of YFP molecules are limited in length due to blinking and photobleaching (5), different time lags between subsequent images, ranging from 6.25 to 150 ms, were used for each experimental condition.

Cumulative probability distributions $P(r^2, t_{lag})$ were constructed for every time lag used and fitted to one of two models. The first model, described by the function

$$P\left(r^2, t_{lag}\right) = 1 - \exp\left(-\frac{r^2}{r_0^2\left(t_{lag}\right)}\right), \qquad (1)$$

describes the probability that the Brownian particle starting at the origin will be found within a circle of radius r at time lag t_{lag}. It is described by the mean-squared displacement, $r_0{}^2(t_{lag}) = 4Dt_{lag}$ (21). If the population of molecules studied segregates into two subpopulations of molecules, one with a fast and one with a slow mobility, Eq. 1 becomes

$$P\left(r^2, t_{lag}\right) = 1 - \left[\alpha \times \exp\left(-\frac{r^2}{r_1^2\left(t_{lag}\right)}\right) + (1-\alpha) \times \exp\left(-\frac{r^2}{r_2^2\left(t_{lag}\right)}\right)\right]. \qquad (2)$$

This equation describes the second model, characterized by mean-squared displacements $r_1{}^2$ and $r_2{}^2$, and relative fractions α and $1-\alpha$, respectively (19).

Average values of $r_1{}^2$ and $r_2{}^2$ from two to four individual experiments were then plotted against t_{lag}. These plots revealed the diffusional behavior of the subpopulations. The increased variance seen at increased time lags in these plots (Fig. 2) is a result of the smaller number of (statistically independent) measurements of r^2 (see also Oian et al. (22)).

The plots were fitted, using the standard error of the mean as a weighting factor, by a free diffusion model ($r_i{}^2 = 4D_i t_{lag}$) or by a confined diffusion model, described by

$$r_i^2\left(t_{lag}\right) = \frac{L^2}{3} \times \left[1 - \exp\left(\frac{-12D_0 t_{lag}}{L^2}\right)\right]. \qquad (3)$$

In this model, it is assumed that diffusion is free within a square of side length L surrounded by an impermeable, reflecting barrier, and that the mean-squared displacement depends on L and the initial diffusion constant, D_0 (23). Alternative fit models (as discussed, e.g., in Wieser and Schutz (24)) are possible as well, but to demonstrate the gross differences between the different cell systems, this relatively simple model was chosen.

RESULTS

In vitro: YFP-C10H-Ras in ZF4 cells

The first single-molecule microscopy approach we used in this study was performed in a zebrafish embryonic fibroblast cell line (ZF4 (25)) to compare our data in the zebrafish system to data from previous studies on YFP-C10H-Ras in

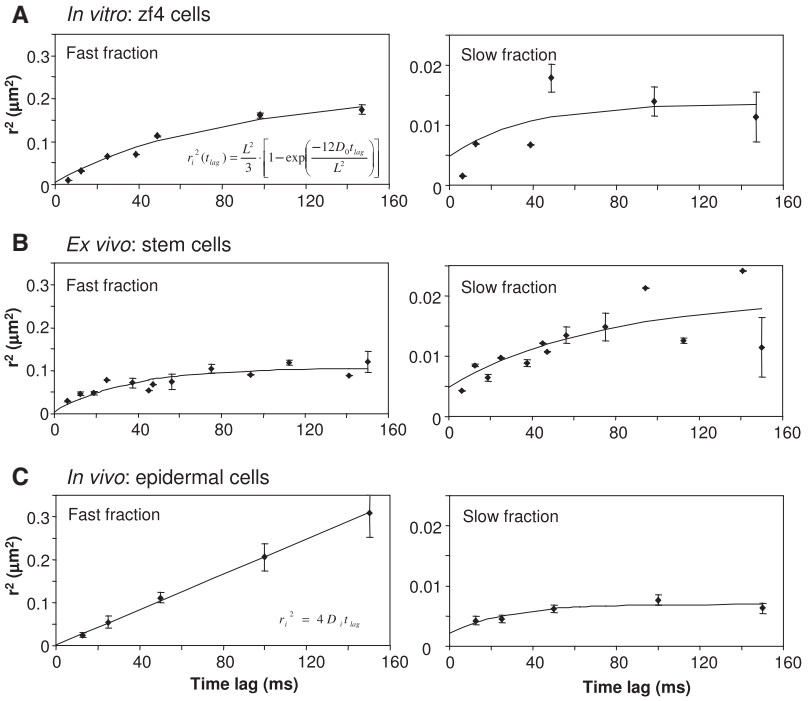

FIGURE 2 Results obtained from squared-displacement distribution analysis (as shown in Fig. 1, *E* and *F*) of data from YFP-C10H-Ras. (*A*) Results from ZF4 cells. (*B*) Results from primary cells. (*C*) Results from epidermal cells. Data of the fast and slow fractions are shown. Mean-squared displacements are plotted against the time lag used (*black diamonds*). Error bars represent the standard error of the mean of two to four individual experiments. Black lines represent curve fits using a confined diffusion or a free diffusion model (for the fast fraction in epidermal cells). The results of all fits are shown in Table 1.

mammalian cell cultures (15,16). The ZF4 cells were transiently transfected with a YFP-C10H-Ras expression plasmid. Confocal laser scanning microscopy showed the fluorescent signal localized predominantly in the membrane (Fig. 1, *A* and *B*), and this localization pattern is in line with previous observations in mammalian cells (15).

Four days after transfection, YFP-C10H-Ras expression levels were significantly decreased, allowing us to observe signals from individual YFP-C10H-Ras molecules in the apical membrane of the cells using a wide-field single-molecule microscopy approach. Diffraction-limited fluorescence intensity peaks were observed (Fig. 1, *C* and *D*). These peaks could be attributed to single molecules, since they showed a width and intensity similar to single YFP fluorescence intensity peaks previously observed using an identical setup (5,15). In addition, the peaks display single-step photobleaching, indicating that they originate from individual YFP molecules. The observed signal/noise ratio (defined as the fluorescence intensity of an individual fluorophore divided by the standard deviation of the background signal (2)) was ~17, resulting in a positional accuracy of ~33 nm in one dimension for the localization of these individual molecules.

Image sequences were acquired using time lags ranging from 6.25 to 75 ms and trajectories of the individual molecules were analyzed (Fig. 1 *E*). For each time lag, between 200 and 3000 trajectories were analyzed, and the squared displacement was calculated for all individual steps of these trajectories. All obtained squared displacements were plotted in a cumulative distribution plot (Fig. 1 *F*), and the data were fitted using a biexponential probability function, indicating the occurrence of two subpopulations of molecules with different diffusion rates. For all time lags used, the relative size of the fractions of these subpopulations (presented as α, the relative size of the fast subpopulation) and the mean-squared displacement (r^2_1 and r^2_2) of the subpopulations were determined. The parameters α, r^2_1, and r^2_2 were plotted as a function of the time lag. The relative fraction size, α, appears to be constant over the range of time lags used and the average size was 0.68 $\pm$ 0.03 (Fig. S1 *A* of the Supporting Material). The mean-squared displacement as a function of the time lag showed asymptotic curves for both fractions (Fig. 2 *A*), indicating that the molecules are not moving freely, that is, that confinement occurs. The data were fitted with a function based on a confined diffusion model, in which the molecules move freely within a square domain of side length L surrounded by an impermeable, reflecting barrier, with initial diffusion constant D_0 (23). The results show an initial diffusion constant (D_0) and domain size (L) of $D_{0,1} = 0.67 \pm 0.08$ $\mu m^2/s$ and $L_1 = 0.79 \pm 0.05$ μm for the fast fraction and $D_{0,2} = 0.06 \pm 0.06$ $\mu m^2/s$ and $L_2 = 0.16 \pm 0.04$ μm for the slow fraction.

Ex vivo: YFP-C10H-Ras in embryonic stem cells

A second single-molecule microscopy approach was performed on primary zebrafish embryonic stem cells. Primary cultures of embryonic cells were obtained by dissociating zebrafish embryos into single cells between 3.5 and 4 h after fertilization (26). At this stage of embryonic development, an embryo consists of several thousands of undifferentiated pluripotent stem cells, which constitute the vast majority of

cells at this stage, covered by a single layer of epithelial cells (27). Upon dissociation, the embryonic cells were kept in culture for several hours (Fig. 3). Transplantation of these cells into donor embryos demonstrated viability and pluripotency of the cultured cells (Fig. S2). To obtain a primary cell culture expressing YFP-C10H-Ras, 100 pg of in vitro transcribed mRNA encoding YFP-C10H-Ras was microinjected into embryos at the one- to two-cell stage. YFP-C10H-Ras expression and membrane localization in the resulting cell culture was confirmed by confocal microscopy (Fig. 3 *D*).

Single-molecule microscopy was performed on these stem cells between 1 and 3 h after embryo dissociation. The signal/noise ratio was ~21, resulting in a positional accuracy of ~30 nm. Time lags between 6.25 and 75 ms were used and at each time lag, between 200 and 1000 trajectories were obtained. Similar to the data found in the ZF4 cells, two populations were detected and the relative size of the fast fraction was 0.67 ± 0.02 (Fig. S1 *B*). The mean-squared displacement plots of both the fast and slow fractions again showed an asymptotic behavior (Fig. 2 *B*), and fitting the data with the confined diffusion model function resulted in $D_{0,1} = 0.72 \pm 0.14\ \mu m^2/s$ and $L_1 = 0.55 \pm 0.03\ \mu m$ for the fast fraction and $D_{0,2} = 0.05 \pm 0.02\ \mu m^2/s$ and $L_2 = 0.21 \pm 0.04\ \mu m$ for the slow fraction.

In vivo: YFP-C10H-Ras in 2-day-old zebrafish embryos

The third single-molecule approach was performed using entire living zebrafish embryos. When zebrafish embryos injected with YFP-C10H-Ras mRNA at the one- to two-cell stage were investigated using our wide-field single-molecule microscopy setup, the signal from the out-of-focus fluorescence was too high to detect signals from individual YFP molecules in the field of focus (data not shown). Furthermore, when cells from YFP-C10H-Ras-expressing embryos were transplanted into wild-type donor embryos, detection of single YFP molecules in the transplanted cells was prevented by the high level of autofluorescence in the donor embryo. For example, the autofluorescent signal in embryos 8 h post-fertilization was three to five times higher than the autofluorescence in ZF4 cells (data not shown). Therefore, fluorescent molecules with a quantum yield three to five times higher than that of YFP should be used in these embryos to get a satisfactory signal/noise ratio.

Since a fluorescent protein molecule with such characteristics is not available, an alternative spectroscopic approach was used to perform single-molecule microscopy in living embryos. A TIRF microscopy setup was used in which an evanescent excitation field at the coverglass-specimen interface excites molecules within <100 nm of the coverglass without exciting molecules in other focal planes. To perform this TIRF-based approach, embryos injected with YFP-C10H-Ras mRNA were used at 2 days after fertilization, and skin cells in the tail region of these embryos were studied (Fig. 4). We decided to use this region and this stage of embryonic development for three reasons. First, the tissue of the tail region is relatively solid at this stage, which makes it possible to add a thin sheet of agarose on top of this part of the embryo without damaging the tissue (which happens when earlier-stage embryos are used). The agarose sheet is needed to press the zebrafish tail against the coverglass and thus position the apical membranes of the outer cell layer of the embryo's skin within the evanescent field. Second, this

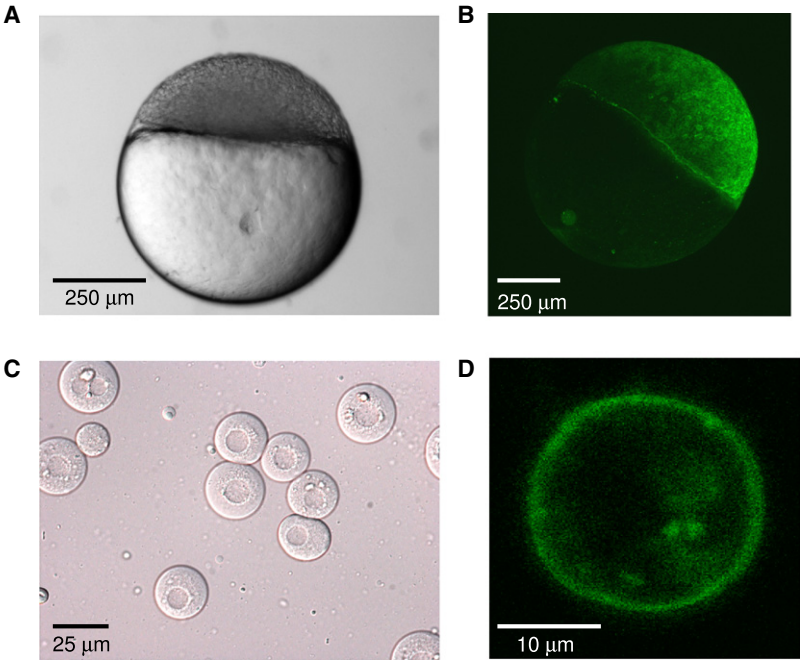

FIGURE 3 The generation of a primary embryonic stem cell culture expressing YFP-C10H-Ras. (*A*) Light microscopy image of a zebrafish embryo at "sphere" stage, between 3.5 and 4 h after fertilization. At this stage, embryos were dissociated into individual cells to generate a primary cell culture. (*B*) Confocal microscopy image of the sphere-stage zebrafish embryos injected with YFP-C10H-Ras mRNA at the one- to two-cell stage. (*C*) Primary stem cell culture derived from sphere-stage embryo. The image was taken using differential interference contrast microscopy. (*D*) Confocal microscopy image of primary zebrafish embryonic stem cell expressing YFP-C10H-Ras. This cell was derived from an embryo, as shown in *B*, and kept in culture for 1 h before the image was taken.

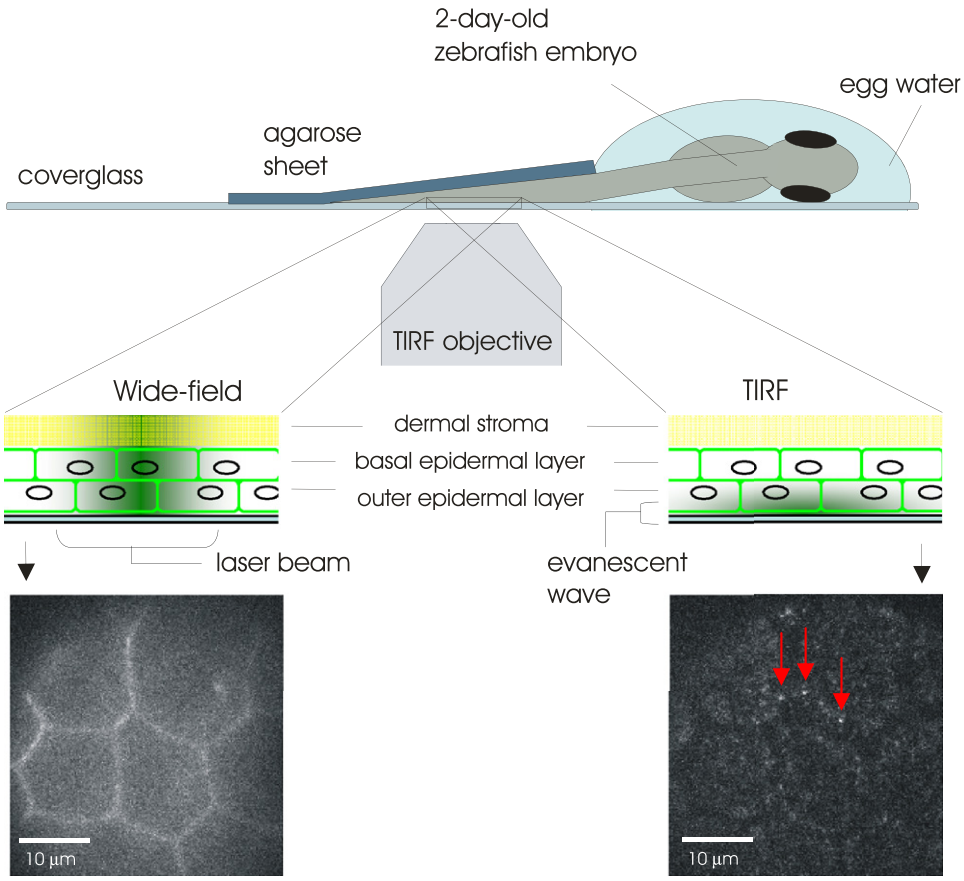

FIGURE 4 Single-molecule microscopy using a living zebrafish embryo. A 2-day-old embryo injected with YFP-C10H-Ras mRNA was placed on a coverslip in a drop of egg water. A sheet of agarose 0.75 mm thick was placed over the embryo covering the tail region, and the coverslip was mounted on a microscopy setup suitable for wide-field and TIRF microscopy. In the left part of the figure, a wide-field microscopic picture of the outer layer of the epidermis is shown, displaying membrane localization of the fluorescent signal. On the right, the acquisition of an image of the same region by TIRF microscopy is shown. Three examples of fluorescence intensity peaks that can be attributed to individual YFP molecules are indicated in the resulting image by red arrows.

outer cell layer of the skin (the superficial stratum) is a homogenous layer of living cells. The homogeneity of this layer was illustrated by confocal microscopic images of 2-day-old embryos of a transgenic zebrafish line expressing GFP-C10H-Ras in all cells (Fig. 5, *C–E*). This layer of cells forms the upper part of the skin (the epidermis) together with an underlying cell layer (28). Third, 2 days after injection of YFP-C10H-Ras mRNA, the expression of this protein is still high enough to visualize these molecules, whereas at later stages the expression disappears due to degradation of the injected mRNA.

Using this approach resulted in a signal/noise ratio of ~29, which is significantly higher than the ratios previously observed using the wide-field fluorescence microscopy setup. As a result, the positional accuracy was improved to ~23 nm. For each embryo, at least 500 trajectories were obtained per time lag. As previously observed in the ZF4 cells and in the primary embryonic cells, two subpopulations of molecules were detected. The size of the fast fraction, α, was 0.75 $\pm$ 0.03 (Fig. S1 *C*). We were surprised to find that the curve representing the mean-squared displacements of the fast fraction displayed a linear increase with time;, and this curve was therefore fitted with a function based on a free diffusion model. It was characterized by a diffusion constant, $D_1 = 0.51 \pm 0.03$ $\mu m^2/s$ (Fig. 2 *C*). This was not an artifact of the TIRF-based approach, since studying embryonic stem cells with this approach showed diffusion behavior of the fast fraction similar to that observed using the wide-field microscopy technique (data not shown). The mean-squared displacement plot of the slow fraction revealed asymptotic behavior relatively close to the offset (0.0022 μm^2), indicating confined diffusion in a relatively small domain (size determined as $L_2 = 0.12 \pm 0.01$ μm). The initial diffusion constant of the slow fraction calculated was $D_{0,2} = 0.04 \pm 0.01$ $\mu m^2/s$ (Fig. 2 *C*).

DISCUSSION

In this study, we performed single-molecule microscopy studies in the zebrafish system using three different approaches. We studied the diffusion pattern of single YFP-C10H-Ras molecules in a zebrafish fibroblast cell line (ZF4 cells), in primary embryonic stem cells, and in cells of the outer layer of the epidermis of living embryos. In Table 1, an overview is presented of the results of this study and those of a previous study in human embryonic kidney (tsA201) cells (15). In all cell types, two subpopulations of molecules were observed, with the fast fraction always constituting 60–75% of the total population. The observed (initial) diffusion constants of the fast fractions were between 0.5 and 0.7 $\mu m^2/s$, whereas those of the slow fraction were ~10-fold lower. The most profound differences between the various

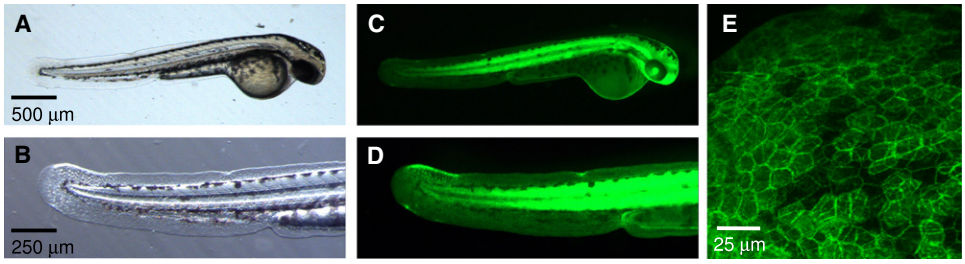

FIGURE 5 Two-day-old zebrafish embryo of a transgenic fish line expressing GFP-C10H-Ras in all cells. (*A*) Transmitted light microscopy image of whole embryo. (*B*) Transmitted light microscopy image of the tail region. (*C*) Fluorescence microscopy image of the whole embryo. (*D*) Fluorescence microscopy image of the tail region. (*E*) Confocal microscopy image of the skin of the tail region. The image shows that the outer cell layer of the epidermis consists of a homogeneous cell population.

cell systems are found in the confinement of the molecules. For example, in the epidermal cells of living embryos, the fast fraction showed free diffusion, as was the case for this fraction in tsA201 cells (15). However, in ZF4 cells and stem cells, this fraction displays confinement in domains of 790 and 550 nm, respectively. The slow fraction shows confinement in all systems, but the size of the domain varies from 120 nm in the epidermal cells to 210 nm in primary zebrafish cells and 250 nm in tsA201 cells.

Thus, we have found two types of membrane domains that confine the lateral diffusion of a membrane-anchored protein: a relatively small domain (120–210 nm) that is present in all cell types studied but differs in size between cell types, and a larger domain (550–790 nm) that is not present in all cell types. These data are in line with previous findings from the Kusumi lab (for a review, see Kusumi et al. (1)). Two types of domains confining the diffusion of the phospholipid DOPE were found in normal rat kidney cells (29): one of 230 and one of 750 nm. In other cell types, the larger domain confining DOPE was not observed, but the occurrence of the smaller domains was detected in all cell types studied, although its size varied dramatically (30). Similar data were found for the transferrin receptor (29) and the μ-opioid receptor (31), both of which are transmembrane proteins, suggesting that these diffusion parameters are mainly specified by the cell type and not by the nature of the membrane molecule. Since the DOPE diffusion was only affected after disruption of the cytoskeleton, these data led to the so-called ''fence and picket'' model, in which transmembrane proteins (''pickets'') that are anchored to the cytoskeleton (''fence'') act as diffusion barriers for all molecules in both leaflets of the plasma membrane (1). It is hypothesized that the function of these diffusion barriers is to confine a cytoplasmic signal to a region in which an extracellular signal is received. This type of membrane compartmentalization can be particularly important in specific cell types or during specific events, e.g., during polarization events or during chemotaxis. Therefore, the need to confine a certain signal to a specific area in the cell may underlie the differences in membrane organization observed between the different cells used in this study.

TABLE 1 Results of YFP-C10H-Ras diffusion analysis

	ZF4 cells	Stem cells	Epidermal cells	tsA201 cells[†]
$D_1(\mu m^2/s)$	0.67 ± 0.08	0.72 ± 0.14	0.51 ± 0.01	0.53 ± 0.02
L_1 (μm)	0.79 ± 0.05	0.55 ± 0.03	NA	NA
D_2 ($\mu m^2/s$)	0.06 ± 0.06	0.05 ± 0.02	0.04 ± 0.01	0.06 ± 0.01
L_2 (μm)	0.16 ± 0.04	0.21 ± 0.04	0.12 ± 0.01	0.25 ± 0.04
α	0.68 ± 0.03	0.67 ± 0.02	0.75 ± 0.03	0.73 ± 0.05

D_1 and D_2 are the (initial) diffusion coefficients obtained for the fast and slow fractions, respectively, when plots representing the mean-squared displacement as a function of the time lag were fitted to a free or confined diffusion model. L_1 and L_2 are the domain sizes obtained when a confined model was used. Values represent the mean ± standard error obtained from the fitting procedure. NA, not applicable.

[†]Data from Lommerse et al. (15).

It has been demonstrated that H-Ras is localized in so-called lipid rafts, microdomains in the plasma membrane that are enriched in cholesterol, sphingolipids, and glycosphingolipids and are ~44 nm in diameter (32). This localization appears to be dependent on the membrane anchor (33). However, for three reasons it is unlikely that organization in these domains underlies the results presented in this study. First, the membrane anchor of K-Ras, a protein molecule known to be absent from lipid rafts, shows diffusion characteristics similar to those of the H-Ras membrane anchor after fusion to YFP (15). Second, cholesterol depletion does not alter the diffusion of YFP-C10H-Ras in tsA201 cells (15), although this effect may differ among cell types. Third, the positional accuracy of the single-molecule microscopy technique used is 23–35 nm, so possible confinement in domains like lipid rafts, with a diameter size of 40–50 nm, is beyond the detection limit (15,16).

By studying cells in the skin of living zebrafish embryos, we successfully extended application of single-molecule microscopy to the level of a living vertebrate organism. Using this approach, we showed that the occurrence of two subpopulations of molecules and the existence of membrane domains in which specific subpopulations are confined are not artifacts that exist only in cultured cells, but are phenomena that occur in cells within the physiological context of a living organism. We thereby corroborate the biological relevance of earlier observations of molecular dynamics of several membrane proteins in cell cultures (1,15). However, we also show that large differences occur between various cell types and systems with respect to the size of the specific membrane domains in which these subpopulations are confined. We

therefore recommend the use of living organisms to make a physiologically relevant determination of the size of these domains. In this study, we present a versatile method of enabling such measurements.

Finally, a plethora of applications are enabled by our in vivo single-molecule microscopy approach. This method can be applied to other membrane proteins, and can even be extended to cytoplasmic or nuclear proteins, e.g. using the highly inclined thin illumination technology (34). In addition, using transgenic zebrafish lines that stably express fluorescent fusion proteins, investigations can be done at later time points. Given the great versatility of the zebrafish model system and the large number of physiological and pathological processes that can be studied in the skin, there are many opportunities for studying these processes. For example, there are zebrafish model systems for skin cancer (35), the human skin condition psoriasis (36), wound healing and regeneration of the skin (37). Studying the dynamics of individual signaling molecules in epidermal cells in these model systems, combined with the opportunities for genetic manipulation of zebrafish embryos, may shed new light on the molecular mechanisms underlying several pathophysiological processes.

SUPPORTING MATERIAL

Two figures are available at http://www.biophysj.org/biophysj/supplemental/S0006-3495(09)01052-2.

The authors thank Gabby Krens, Annemarie Meijer, Ivo van Laanen, and Saskia Rueb for technical assistance with the zebrafish and cell culture work, and Karin Vastenhoud, Sandra de Keijzer, and Freek van Hemert for assistance with single-molecule microscopy and data analysis.

The authors acknowledge financial support from Cyttron, in the Besluit Subsidies Investeringen Kennisinfrastructuur program (M.S.), and Stichting voor Fundamenteel Onderzoek der Materie (W.K.), which in turn is financially supported by the Nederlandse Organisatie voor Wetenschappelijk Onderzoek.

REFERENCES

1. Kusumi, A., H. Ike, C. Nakada, K. Murase, and T. Fujiwara. 2005. Single-molecule tracking of membrane molecules: plasma membrane compartmentalization and dynamic assembly of raft-philic signaling molecules. *Semin. Immunol.* 17:3–21.
2. Schmidt, T., G. J. Schutz, W. Baumgartner, H. J. Gruber, and H. Schindler. 1996. Imaging of single molecule diffusion. *Proc. Natl. Acad. Sci. USA.* 93:2926–2929.
3. Sako, Y., S. Minoghchi, and T. Yanagida. 2000. Single-molecule imaging of EGFR signalling on the surface of living cells. *Nat. Cell Biol.* 2:168–172.
4. Schutz, G. J., G. Kada, V. P. Pastushenko, and H. Schindler. 2000. Properties of lipid microdomains in a muscle cell membrane visualized by single molecule microscopy. *EMBO J.* 19:892–901.
5. Harms, G. S., L. Cognet, P. H. Lommerse, G. A. Blab, and T. Schmidt. 2001. Autofluorescent proteins in single-molecule research: applications to live cell imaging microscopy. *Biophys. J.* 80:2396–2408.
6. de Keijzer, S., A. Serge, F. van Hemert, P. H. Lommerse, G. E. Lamers, et al. 2008. A spatially restricted increase in receptor mobility is involved in directional sensing during *Dictyostelium discoideum* chemotaxis. *J. Cell Sci.* 121:1750–1757.
7. Harms, G. S., M. Sonnleitner, G. J. Schutz, H. J. Gruber, and T. Schmidt. 1999. Single-molecule anisotropy imaging. *Biophys. J.* 77:2864–2870.
8. Iino, R., I. Koyama, and A. Kusumi. 2001. Single molecule imaging of green fluorescent proteins in living cells: E-cadherin forms oligomers on the free cell surface. *Biophys. J.* 80:2667–2677.
9. Ike, H., A. Kosugi, A. Kato, R. Iino, H. Hirano, et al. 2003. Mechanism of Lck recruitment to the T-cell receptor cluster as studied by single-molecule-fluorescence video imaging. *ChemPhysChem.* 4:620–626.
10. Lommerse, P. H., B. E. Snaar-Jagalska, H. P. Spaink, and T. Schmidt. 2005. Single-molecule diffusion measurements of H-Ras at the plasma membrane of live cells reveal microdomain localization upon activation. *J. Cell Sci.* 118:1799–1809.
11. Blaser, H., S. Eisenbeiss, M. Neumann, M. Reichman-Fried, B. Thisse, et al. 2005. Transition from non-motile behaviour to directed migration during early PGC development in zebrafish. *J. Cell Sci.* 118:4027–4038.
12. Pauls, S., B. Geldmacher-Voss, and J. A. Campos-Ortega. 2001. A zebrafish histone variant H2A.F/Z and a transgenic H2A.F/Z:GFP fusion protein for in vivo studies of embryonic development. *Dev. Genes Evol.* 211:603–610.
13. Niell, C. M., M. P. Meyer, and S. J. Smith. 2004. In vivo imaging of synapse formation on a growing dendritic arbor. *Nat. Neurosci.* 7:254–260.
14. Malumbres, M., and M. Barbacid. 2003. RAS oncogenes: the first 30 years. *Nat. Rev. Cancer.* 3:459–465.
15. Lommerse, P. H., G. A. Blab, L. Cognet, G. S. Harms, B. E. Snaar-Jagalska, et al. 2004. Single-molecule imaging of the H-ras membrane-anchor reveals domains in the cytoplasmic leaflet of the cell membrane. *Biophys. J.* 86:609–616.
16. Lommerse, P. H., K. Vastenhoud, N. J. Pirinen, A. I. Magee, H. P. Spaink, et al. 2006. Single-molecule diffusion reveals similar mobility for the Lck, H-ras, and K-ras membrane anchors. *Biophys. J.* 91:1090–1097.
17. He, S., E. Salas-Vidal, S. Rueb, S. F. Krens, A. H. Meijer, et al. 2006. Genetic and transcriptome characterization of model zebrafish cell lines. *Zebrafish.* 3:441–453.
18. Koopmans, W. J., A. Brehm, C. Logie, T. Schmidt, and J. van Noort. 2007. Single-pair FRET microscopy reveals mononucleosome dynamics. *J. Fluoresc.* 17:785–795.
19. Schutz, G. J., H. Schindler, and T. Schmidt. 1997. Single-molecule microscopy on model membranes reveals anomalous diffusion. *Biophys. J.* 73:1073–1080.
20. Bobroff, N. 1986. Position measurement with a resolution and noise-limited instrument. *Rev. Sci. Instrum.* 57:1152–1157.
21. Anderson, C. M., G. N. Georgiou, I. E. Morrison, G. V. Stevenson, and R. J. Cherry. 1992. Tracking of cell surface receptors by fluorescence digital imaging microscopy using a charge-coupled device camera. Low-density lipoprotein and influenza virus receptor mobility at 4°C. *J. Cell Sci.* 101:415–425.
22. Qian, H., M. P. Sheetz, and E. L. Elson. 1991. Single particle tracking. Analysis of diffusion and flow in two-dimensional systems. *Biophys. J.* 60:910–921.
23. Kusumi, A., Y. Sako, and M. Yamamoto. 1993. Confined lateral diffusion of membrane receptors as studied by single particle tracking (nanovid microscopy). Effects of calcium-induced differentiation in cultured epithelial cells. *Biophys. J.* 65:2021–2040.
24. Wieser, S., and G. J. Schutz. 2008. Tracking single molecules in the live cell plasma membrane: do's and don't's. *Methods.* 46:131–140.
25. Driever, W., and Z. Rangini. 1993. Characterization of a cell line derived from zebrafish (*Brachydanio rerio*) embryos. *In Vitro Cell. Dev. Biol. Anim.* 29A:749–754.
26. Montero, J. A., B. Kilian, J. Chan, P. E. Bayliss, and C. P. Heisenberg. 2003. Phosphoinositide 3-kinase is required for process outgrowth and

cell polarization of gastrulating mesendodermal cells. *Curr. Biol.* 13:1279–1289.

27. Kimmel, C. B., W. W. Ballard, S. R. Kimmel, B. Ullmann, and T. F. Schilling. 1995. Stages of embryonic development of the zebrafish. *Dev. Dyn.* 203:253–310.
28. Le Guellec, D., G. Morvan-Dubois, and J. Y. Sire. 2004. Skin development in bony fish with particular emphasis on collagen deposition in the dermis of the zebrafish (*Danio rerio*). *Int. J. Dev. Biol.* 48:217–231.
29. Fujiwara, T., K. Ritchie, H. Murakoshi, K. Jacobson, and A. Kusumi. 2002. Phospholipids undergo hop diffusion in compartmentalized cell membrane. *J. Cell Biol.* 157:1071–1081.
30. Murase, K., T. Fujiwara, Y. Umemura, K. Suzuki, R. Iino, et al. 2004. Ultrafine membrane compartments for molecular diffusion as revealed by single molecule techniques. *Biophys. J.* 86:4075–4093.
31. Suzuki, K., K. Ritchie, E. Kajikawa, T. Fujiwara, and A. Kusumi. 2005. Rapid hop diffusion of a G-protein-coupled receptor in the plasma membrane as revealed by single-molecule techniques. *Biophys. J.* 88:3659–3680.
32. Prior, I. A., C. Muncke, R. G. Parton, and J. F. Hancock. 2003. Direct visualization of Ras proteins in spatially distinct cell surface microdomains. *J. Cell Biol.* 160:165–170.
33. Rotblat, B., I. A. Prior, C. Muncke, R. G. Parton, Y. Kloog, et al. 2004. Three separable domains regulate GTP-dependent association of H-ras with the plasma membrane. *Mol. Cell. Biol.* 24:6799–6810.
34. Tokunaga, M., N. Imamoto, and K. Sakata-Sogawa. 2008. Highly inclined thin illumination enables clear single-molecule imaging in cells. *Nat. Methods.* 5:159–161.
35. Haldi, M., C. Ton, W. L. Seng, and P. McGrath. 2006. Human melanoma cells transplanted into zebrafish proliferate, migrate, produce melanin, form masses and stimulate angiogenesis in zebrafish. *Angiogenesis.* 9:139–151.
36. Mathias, J. R., M. E. Dodd, K. B. Walters, J. Rhodes, J. P. Kanki, et al. 2007. Live imaging of chronic inflammation caused by mutation of zebrafish Hai1. *J. Cell Sci.* 120:3372–3383.
37. Kawakami, A., T. Fukazawa, and H. Takeda. 2004. Early fin primordia of zebrafish larvae regenerate by a similar growth control mechanism with adult regeneration. *Dev. Dyn.* 231:693–699.